Journal of Materials Chemistry B

Improving the Anti-inflammatory Efficacy of Dexamethasone in the Treatment of Rheumatoid Arthritis with Polymerized Stealth Liposomes as a Delivery Vehicle

Journal:	*Journal of Materials Chemistry B*
Manuscript ID	TB-ART-11-2019-002538.R1
Article Type:	Paper
Date Submitted by the Author:	17-Dec-2019
Complete List of Authors:	Fang, Jiyu; University of Central Florida, Advanced Materials Processing and Analysis Center Wang, Qin ; Southwest Jiaotong University He, Liming ; Southwest Jiaotong University Fan, Donghao ; Southwest Jiaotong University Liang, Wenlang; University of Central Florida, Advanced Materials Processing and Analysis Center

Improving the Anti-inflammatory Efficacy of Dexamethasone in the Treatment of Rheumatoid Arthritis with Polymerized Stealth Liposomes as a Delivery Vehicle

Qin Wang,[a,*] Liming He,[a] Donghao Fan,[a] Wenlang Liang,[a,b] and Jiyu Fang[b,*]

[a] Key Laboratory of Advanced Technologies of Materials, Ministry of Education and School of Materials Science and Engineering, Southwest Jiaotong University, Chengdu 610031, China. Email: Wangqin666@swjtu.edu.cn

[b]Advanced Materials Processing and Analysis Center and Department of Materials Science and Engineering, University of Central Florida, Florida 32816, United State. Email: Jiyu.fang@ucf.edu

Abstract

Rheumatoid arthritis (RA) is an autoimmune disease that causes chronic inflammation of the joints of body. Although liposomes are a promising drug delivery vehicle, there is still a challenge of using conventional liposomes for the treatment of RA due to their short circulation time and physicochemical instability in blood vessels. Here, we report the formation of polymerized stealth liposomes composed of 1,2-bis(10,12-tricosadiynoyl)-sn-glycero-3-phosphocholine ($DC_{8,9}PC$) and 1,2-distearoyl-sn-glycero-3-phospho-ethanolamine-poly(ethyleneglycol) (DSPE-PEG_{2000}) with thin-film hydration method, in which $DC_{8,9}PC$ molecules are cross-linked in the bilayer of the liposomes by UV irradiation and the PEG chains presenting at the surface of the liposomes provide a stealth layer. We demonstrate that the polymerized stealth liposomes are stable and show long circulation time in blood vessels. They can be internalized by cells without significant toxicity. After being injected into arthritic rats, the polymerized stealth liposomes with loaded dexamethasone (Dex) show long blood circulation time and accumulate preferentially in inflamed joints, consequently

suppressing the level of proinflammatory cytokines (TNF-α and IL-1β) in joint tissues, reducing the swelling of inflamed joints and alleviating the progression of RA. We believe that polymerized stealth liposomes can be used as a promise drug delivery vehicle for various therapeutic applications.

Keywords: Rheumatoid arthritis, dexamethasone, liposomes, drug delivery and anti-inflammatory.

1. Introduction

Rheumatoid arthritis (RA) is an autoimmune disease that can cause chronic inflammation of the joints of body.[1] The inadequate control of RA may cause severe joint damage, eventually leading to disability. Dexamethasone (Dex) is an anti-inflammatory drug for the treatment of RA by managing inflammation.[2] In general, adequate doses of Dex in inflamed joints are needed to achieve good anti-inflammatory efficacy. However, the long-term use and high dose of Dex may have severe side effects including osteoporosis, hypertension, muscle wasting, and hyperglycemia. Thus, there has been great interest in developing nanoscale drug delivery vehicles to reduce the non-targeted side effects and enhance the anti-inflammatory efficacy of Dex.[3-6] In RA, the wall of blood vessels becomes "leaky" in the inflamed joints.[7] The extravasation of nanoscale drug delivery vehicles through the leaky vasculature and subsequent inflammatory cell-mediated sequestration (ELVIS), a "passive targeting mechanism", allows them to accumulate preferentially in the inflamed joints and achieve enhanced anti-inflammatory efficacy.[8]

Liposomes, a small phospholipid vesicle consisting of lipid bilayers enclosing a discrete aqueous core, are a well-known nanoscale drug delivery vehicle for reducing the toxicity of drugs.[9-12] As a drug delivery vehicle, liposomes offer several advantages including biocompatibility, capability of encapsulating both lipophilic and hydrophilic drugs, and tunable sizes and physicochemical properties. Despite these advantages, there are two major obstacles facing the therapeutic application of conventional liposomes made up of phospholipid bilayers. First, the blood circulation time of

conventional liposomes is limited because they can be rapidly taken up by the reticuloendothelial system (RES) in the liver.[13-14] Polyethylene glycol (PEG) is an effective hydrophilic polymer for providing "stealth" properties at the surface of liposomes to reduce the recognition and uptake by the RES, consequently increasing the circulation time of liposomes in vivo.[15-20] Second, conventional liposomes often lack the long-term stability in physiologic conditions, which leads to the leakage of the encapsulated drugs at non-target sites. The instability of liposomes may be caused by osmotic rupture, lipid hydrolysis, and surfactant-induced disintegration.[21-22] The polymerization of lipids in the bilayers has been proven to be an effective approach to achieve the structural integrity of liposomes.[23-27] Although there were few reports in the design of polymerized stealth liposomes by combining these two approaches,[26-27] their applications as a drug delivery vehicle were still limited in vivo.

In this paper, we prepared polymerized stealth liposomes composed of 1,2-bis(10,12-tricosadiynoyl)-sn-glycero-3-phosphocholine ($DC_{8,9}PC$) and 1,2-distearoyl-sn-glycero-3-phospho-ethanolamine-poly(ethyleneglycol) (DSPE-PEG_{2000}) with thin-film hydration method, in which $DC_{8,9}PC$ molecules were cross-linked in the bilayer by UV irradiation to improve the structural integrity of the liposomes and the PEG chains provided a stealth layer to enhance their blood circulation time in blood vessels. The formation and stability of polymerized stealth liposomes were studied by dynamic light scattering (DLS) and transmission electron microscopy (TEM). The biocompatibility and cellular uptake of polymerized stealth liposomes were evaluated in vitro with MTT assays and flow cytometry measurements, respectively. After

arthritic rats were treated with polymerized stealth liposomes, we used liquid chromatography-mass spectrometry and IVIS® Spectrum to study their pharmacokinetics and biodistribution. Furthermore, the therapeutic effect of polymerized stealth liposomes with loaded Dex in the treatment of RA was verified by measuring the reduction of the joint score, the paw thickness, and the level of inflammatory cytokines (TNF-α and IL-1β) in the serum and joint tissues of arthritic rats as well as analyzing the histological pathology of ankle joints.

2. Experimental section

Materials and reagents. 1,2-bis(10,12-tricosadiynoyl)-sn-glycero-3-phosphocholine ($DC_{8,9}PC$) and 1,2-distearoyl-sn-glycero-3-phospho-ethanolamine-poly(ethyleneglycol) (DSPE-PEG_{2000}) were purchased from Avanti Polar Lipids (Alabaster, USA). Dexamethasone (Dex), coumarin-6 (cou-6), and 1,1'-dioctadecyl-3,3,3',3'-Tetramethylindodicarbocyanine (DiD) were obtained from Sigma Aldrich (Saint Louis, MO, USA). Freund's complete adjuvant was from Chondrex (Washington DC, USA). Rat TNF-α and IL-1β Elisa Kit was from Dakewei (Beijing, China). Lipopolysaccharide (LPS), 3-(4,5-dimethylthiazol-2-yl)-2,5-diphenyltetrazolium bromide (MTT), and Triton X-100 were purchased from Aladdin (Shanghai, China). All other chemicals were obtained from Kelong (Sichuan, China). Male SD rats with the weight of 160-180 g were purchased from the Experimental Animal Center of Dashuo (Sichuan, China). Animal experiments were carried out in strict according to the recommendations in the U.S. National Institutes of Health Guide for the Care and

Use of Laboratory Animals. All animal experiments were approved by the Institutional Animal Care and Ethics Committee of Southwest Jiaotong University.

Liposome preparation: Liposomes were formed with a thin-film hydration method. Briefly, $DC_{8,9}PC$ and DSPE-PEG_{2000} with different mixed ratios were dissolved in a mixed organic solvent consisted of methanol and chloroform at a molar ratio of 1:1, followed by the evaporation process under vacuum until a dry thin film was formed. Afterwards, 2 mL PBS solution with pH 7.4 was added to hydrate the thin film. The obtained solution was subjected to ultrasonication for 5 min, then passed through a 0.45 μm filter to yield a final liposome formulation. The polymerization of liposomes was carried out by UV irradiation (254 nm) for 2 h.

Liposome characterization: The size, polydispersity index (PDI) and zeta potential of liposomes were analyzed using Zetasizer Nano ZS90 dynamic light scattering (DLS) (Malvern, UK). Transmission electron microscopy (TEM) measurements were performed with a JEOL TEM-1011 operated at 200 kV. Differential scanning calorimetry (DSC, TA Instrument, USA) was used to measure the phase-transition of liposomes.

Liposome Stability: The stability of liposomes was studied in aqueous solution with or without Triton X-100 (20 μM) at room temperature by measuring their sizes and polydispersity index (PDI) values at different time intervals with dynamic light scattering (DLS).

Dex encapsulation: Dexamethasone (Dex) at the concentration of 1mg/mL was mixed with $DC_{8,9}PC$ and DSPE-PEG_{2000} in the 1:1 mixture of methanol and chloroform. The

subsequent procedure was carried out as abovementioned. The entrapment efficiency and loading of Dex in the bilayer of liposomes were determined using an ultrafiltration tube (molecular weight cut-off: 100 kDa). Unencapsulated Dex was quantified with high-performance liquid chromatography (Agilent, CA, USA). Encapsulation efficiency and Dex loading yield were determined using the following formulas:

$$\text{Encapsulation rate (\%)} = \frac{Weigth\ of\ \text{encapsulated}\ Dex\ in\ \ liposomes}{Weight\ of\ the\ feeding\ Dex} \times 100\%$$

$$\text{Dex loading yield (\%)} = \frac{Weight\ of\ encapsulated\ Dex\ in\ liposomes}{Total\ weight\ of\ the\ liposomes\ formulations} \times 100\%$$

Leakage of Dex from liposomes in serum: Liposomes with loaded Dex were incubated with rat serum in a shaker at the speed of 70 rpm at 37°C for 4 h. Afterwards, the samples were centrifuged at 1000 g for 30 min. The percentage of Dex leakage in the supernatant was quantified using a HPLC method.

In vitro release of Dex from liposomes: The release behavior of Dex from liposomes in vitro was investigated using the dialysis method. Briefly, free Dex or Dex-loaded liposomes (500 μL) were added into dialysis bags with a molecular weight cut-off of 10 kDa. Dialysis bags were immersed in 50 mL PBS solution at pH 7.4 and incubated for a period of time at 37 °C in a shaker at 70 rpm. At the indicated time points, an aliquot (100 μL) of the external medium was taken out, and the same volume of fresh PBS solution with pH 7.4 was replenished. The released Dex in the medium was measured using a HPLC method.

Cell lines and culture: The murine macrophage Raw264.7 cell line and human umbilical vein endothelial cell (HUVEC) cell line were obtained from the American

Type Culture Collection (Rockville, MD, USA). Both Raw264.7 and HUVEC were cultured in Dulbecco's modified Eagle medium containing 10% fetal bovine serum, 100 U/mL penicillin, and 100 mg/mL streptomycin (Kaiji, Sichuan, China). These cells were incubated at 37 °C in a humidified atmosphere of 5% CO_2.

Cell viability: MTT assay was used for evaluate the cell viability of liposomes. Raw 264.7 and HUVEC cells were seeded into a 96-well microplate at the density of 1×10^4 cells per well and cultured overnight. Then cells were incubated with liposomes at concentrations ranging from 25 to 200 μg/mL. Finally, MTT solution (5 mg/mL) was added and incubated with cells for 4 h. The medium was removed and DMSO (100 μL) was added to each well to dissolve the formazan crystals. Absorbance (490 nm) of all samples were measured with a microplate reader (Thermo, USA). Relative cell viability was calculated using the following formula:

$$\text{Cell viability} = \frac{A_{sample} - A_{blank}}{A_{negative\ control} - A_{blank}} \times 100\%.$$

Cellular uptake: Raw 264.7 were seeded into a 12-well microplate (5×10^5 cells) without or with lipopolysaccharide (LPS) having the concentration of 0.1 μg/mL. For flow cytometry and fluorescence microscopy measurements, coumarin-6 (Cou-6) was loaded in liposomes during their formation. Free Cou-6 or Cou-6-loaded liposomes were incubated with Raw 264.7 for 1 h. PBS was then added to wash each well and remove non-internalized liposomes. Finally, cellular uptake was assessed using flow cytometry (Cytomics FC500, Beckman Coulter, Miami, FL, USA) and fluorescence microscopy (Olympus, Japan).

Adjuvant-induced arthritis model: The SD rats were intraplantarly injected with 100 μL complete Freund's adjuvant (M. tuberculosis H-37RA 10 mg/mL) at hind paws (Day 0). The progression of the joint inflammation and swelling was monitored daily. During disease progression, adequate care was given to ensure that rats have access to food and water.

Pharmacokinetics study: SD rats were injected with Dex-loaded liposomes at a dosage of 2 mg/kg via tail vein. At the indicated time points, 0.4 ml of blood was collected through orbit with a 0.5-mm capillary tube and then centrifuged at the 5000 rpm for 10 min to obtain plasma samples. To determine Dex concentrations, plasma samples were extracted twice via methyl tertbutyl ether and analyzed using liquid chromatography-mass spectrometry (LC-MS/MS, 1200 series, Agilent Technologies, USA). Dex (MW 392.3 Da) was detected at the m/z transition 392.3→354.0. Pharmacokinetic parameters in terms of half-life and AUC (area under the concentration-time curves) were calculated using DAS2.0.

Biodistribution: In order to visually analyze the biodistribution behavior of liposomes using the living imaging method, the hydrophobic infrared fluorescent dye DiD was encapsulated into liposome. Arthritic rats were intravenously administrated with free DiD or DiD-loaded liposomes at an equal dosage of 2 μg DiD per rat. At 2, 6 and 24 h after injection, rats were sacrificed and their major organs were collected. Fluorescence intensity of collected tissues was analyzed using the IVIS® Spectrum system (Caliper, Hopkington, MA, USA). Untreated rats were served as blank controls.

Therapeutic efficacy evaluation: Arthritic rats were randomly divided into three groups,

which were injected with PBS, free Dex, Dex-loaded liposomes via tail vein on day 12, 14 and 16 after arthritis induction, respectively. Dex dose was 1 mg/kg at each group. Pharmacodynamics assessments were proceeded for 8 consecutive days from Day 12. Healthy rats without receiving any treatment served as a naive control. Joint scores and hind paw thicknesses were measured. On day 19 after induction, blood and joint tissues were collected from each group. The level of the pro-inflammatory cytokines (TNF-α and IL-1β) in serum and homogenate from joint tissues was measured with enzyme-linked immunosorbent assay (ELISA). After the treatment, ankle joints were dissected and fixed in 4% paraformaldehyde. After the decalcification in 15% neutral EDTA solution for 25 days at 25 °C, joint tissue was subjected to hematoxylin-eosin stanning. The histological score was determined by grading the cellular infiltrates and cartilage erosion from 0 to 3, where 0 = no; 1 = mild (1%–10%); 2 = moderate (11%–50%); 3 = severe (51%–100%). Hematological examinations were also carried out on the day 19. Blood was collected from rats. White blood cells, red blood cells, and platelets were counted.

Statistical analysis: Statistical analysis was conducted with GraphPad Prism (7.0). Statistical significances were assessed with Student t-test and one-way ANOVA. The significance was defined as follows: *P < 0.05, **P < 0.01, and ***P < 0.001.

3. Results and discussion

3.1. Synthesis and characterization

The chemical structure of $DC_{8,9}PC$ and DSPE-PEG_{2000} is shown in Fig. 1a and 1b, respectively. DSPE-PEG_{2000} has a PEG chain which is covalently linked to a

distearoyl lipid tail. $DC_{8,9}PC$ contains diacetylene groups within its tails, which can be cross-linked by UV irradiation.[28] It was reported that the polymerization of $DC_{8,9}PC$ in the bilayers could significantly enhance the structural integrity of $DC_{8,9}PC$ liposomes.[29] In our experiments, polymerized stealth liposomes were formed at the different mixed molar ratios of $DC_{8,9}PC$ and DSPE-PEG_{2000} with thin-film hydration method (Fig. 1c), followed by UV irradiation (Fig. 1d). The resultant $DC_{8,9}PC$/DSPE-PEG_{2000} liposome solution appeared white in color prior to UV irradiation, but turned orange color after UV irradiation, suggesting that the cross-linking of $DC_{8,9}PC$ in the bilayer of the liposomes occurred.[24] The orange color of polymerized stealth liposome solution turned lighter as the increase of the molar fraction of DSPE-PEG_{2000} (Fig. 2a) due to the decrease of the cross-linked density of $DC_{8,9}PC$ in the bilayer of the liposomes. The polymerized stealth liposomes with 10 mol% DSPE-PEG_{2000} showed a single endothermic peak with the phase transition temperature at ~ 47 °C (Fig. 2b), which was close to the transition temperature of pure $DC_{8,9}PC$ liposomes,[24] but higher than that of pure DSPE-PEG_{2000} micelles with the melting transition at 12.8°C.[30] The single endothermic peak suggested the well-mixed $DC_{8,9}PC$ and DSPE-PEG_{2000} components in the bilayer of polymerized stealth liposomes. With the increase of DSPE-PEG_{2000}, the endothermic peak slightly shifted to low temperature ranges. When DSPE-PEG_{2000} was over 50 mol%, polymerized stealth liposomes showed two separate endothermic peaks (Fig. 2b), suggesting the phase separation of $DC_{8,9}PC$ and DSPE-PEG_{2000} components within the bilayer. In addition, we noted that the hydrodynamic size and polydispersity index (PDI) value of polymerized stealth liposomes increased with the

increase of mole% DSPE-PEG_{2000}, (Fig. 2c).

In comparison with the polymerized stealth liposomes with 25 mol%, 50 mol% and 90 mol% DSPE-PEG_{2000}, the polymerized stealth liposomes with 10 mol% DSPE-PEG_{2000} were more stable with a higher phase transition temperature. It was reported that smaller liposomes were more easily pass through the leaky vasculature in the inflamed sites to achieve passive targeting than larger liposomes in vivo.[31-32] Thus, we used the polymerized stealth liposomes with 10 mol% DSPE-PEG_{2000} as a drug delivery vehicle for the treatment of RA. The hydrodynamic size of stealth liposomes with 10 mol% DSPE-PEG_{2000} was slightly reduced by UV polymerization, but their surface charge remained nearly changed (Fig. 3a). TEM images revealed that the stealth liposomes maintained a spherical shape after UV polymerization (Fig. 3b). Interestingly, the encapsulation rate and loading yield of polymerized stealth liposomes for Dex were significantly higher than that of nonpolymerized stealth liposomes (Fig. 3a). Due to the hydrophobic nature, the solubility of Dex in aqueous solution at room temperature is expected to be low. We noted that 2h UV-irradiation could raise the temperature of Dex solution from 25 °C to 41°C, which could increase the solubility of Dex in aqueous solution. It was reported that the photopolymerization of $DC_{8,9}PC$ caused the formation of small pores in the bilayer of liposomes.[26] Thus, the solubilized Dex molecules by UV-irradiation are expected to penetrate into the small pores of polymerized stealth liposomes, consequently leading to the increase of the encapsulation rate and loading yield.

3.2. Stability and in vitro release

Both polymerized and nonpolymerized stealth liposomes with 10 mol% DSPE-PEG_{2000} were stable in aqueous solution at room temperature. Their hydrodynamic sizes remained nearly unchanged for 7 days (Fig. 3c). Among various surfactants, Triton X-100 was known to be able to disrupt lipid membranes.[33] Thus, we verified the stability of both polymerized and nonpolymerized stealth liposomes in the presence of Triton X-100. An increase in the hydrodynamic size of nonpolymerized stealth liposomes was observed even after 5 min incubation with Triton X-100 at the concentration of 20 μM. 30 min incubation caused a significant increase in the hydrodynamic size of nonpolymerized stealth liposomes (Fig. 3d), suggesting the disruption of nonpolymerized stealth liposomes by Triton X-100. In contract, there was only a slight increase in the hydrodynamic size of polymerized stealth liposomes after 30 min incubation with 20 μM Triton X-100 (Fig. 3d). When entering blood circulation, liposomes often meet with the leakage of drugs before they are able to reach to diseased sites because serum lipoproteins can potentially interact with the lipid bilayer of liposomes and consequently disrupt them,[34-35] which limits their applications as a drug delivery vehicle in vivo.[36] Therefore, we tested the leakage of Dex from both polymerized and nonpolymerized stealth liposomes in rat serum. After 4h incubation with rat serum at 37 °C, we found that less than 5% Dex was leaked out from polymerized stealth liposomes, but almost 60% Dex was leaked out from nonpolymerized stealth liposomes (Fig. 3e). Our results demonstrate that polymerized

stealth liposomes have a higher degree of resistance to the disruption of Triton X-100 and serum lipoproteins than nonpolymerized stealth liposomes, which will be beneficial in the targeting treatment of RA. Fig. 3f shows the release profiles of Dex from polymerized and nonpolymerized stealth liposomes in PBS solution at 37 °C. The slow release kinetics of Dex from polymerized stealth liposomes was observed with ~ 10% Dex released after 6 h, followed by a sustained release. In contrast, more than 70% Dex was released from nonpolymerized stealth liposomes at first 6 h.

3.3. In vitro cytotoxicity and cellular uptake

To evaluate the biocompatibility of polymerized stealth liposomes with 10 mol% DSPE-PEG_{2000}, we studied their cytotoxicity against Raw 264.7 murine macrophages and human umbilical vein endothelial cells (HUVEC) cells. They showed no significant affect on the viability of Raw 264.7 and HUVEC cells at the concentration as high as 200 μg/mL (Fig. 4a and 4b). To explore the uptake of polymerized stealth liposomes under inflammatory conditions, lipopolysaccharide (LPS) was used as a stimulus to activate Raw264.7 to an inflammatory state. In our experiments, Couramin-6 (Cou-6, a fluorescent dye) was used to replace Dex. Free Cou-6 or polymerized stealth liposomes with loaded Cou-6 were incubated with LPS-activated or nonactivated Raw 264.7 for 1 h. The uptake by Raw264.7 was examined using flow cytometry measurements and fluorescence microscopy. As can be seen in Fig. 4c, the uptake of free Cou-6 by Raw 264.7 was minimal with and without LPS activation. Whereas the uptake of polymerized stealth liposomes with loaded Cou-6 was substantially enhanced, especially when Raw 264.7 was in the inflammatory state. The fluorescence

microscopy images shown in Figure 4d further confirmed the results from the flow cytometry measurements. The polymerized stealth liposomes were able to facilitate cellular endocytosis. The activated Raw 264.7 was more efficient in phagocytosing the polymerized stealth liposomes than the non-activated Raw 264.7.

3.4. Pharmacokinetics and biodistribution

In pharmacokinetic studies, polymerized or nonpolymerized stealth liposomes with Dex at a dosage of 2 mg/kg were injected intravenously to healthy rats. The plasma concentration of Dex was measured with liquid chromatography-mass spectrometry (LC-MS/MS) at different time intervals. Fig. 5a shows the concentration-time curves. The area under the concentration-time curve (AUC0→t) of polymerized stealth liposomes was higher than that of nonpolymerized stealth liposomes (Fig. 5b), suggesting that Dex loaded in the polymerized stealth liposomes had higher bioavailability than that in the nonpolymerized liposomes. The half time ($T_{1/2}$) in the elimination phase of polymerized stealth liposomes was 1.74-fold higher than that of non-polymerized stealth liposomes (Fig. 5b). This result confirms that polymerized stealth liposomes had a longer circulation time than nonpolymerized stealth liposomes due to their higher stability in vivo. It was reported that drug delivery vehicles with the slower drug release kinetics and the longer duration of therapeutic activity resulted in better joint protection.[37] Thus, polymerized stealth liposomes were used in our further experiments.

Fig. 5c shows the fluorescence images of arthritic rats after the intravenous injection of free DiD (a fluorescent dye) or polymerized stealth liposomes with loaded

DiD. Naive rats were used as a control group to deduct the autofluorescence of rats. There was no fluorescence observed in arthritic rats after the injection of free DiD, suggesting the rapid elimination of free DiD by body. However, the fluorescence in inflamed joints was visible only 2 h after the injection of polymerized stealth liposomes with loaded DiD, become stronger after 6 h, and persisted more than 12 h after the injection. At indicated time points, all the rats were sacrificed. Their primary organs and hind limbs were subjected to ex vivo imaging. For the rats treated with free DiD, fluorescence mainly came from the liver and was negligible in hind limbs (Fig. 5d). While for the rats treated with polymerized stealth liposomes with loaded DiD, intensive fluorescence was first observed in limbs (Fig. 5d). Over time, fluorescence appeared in liver and spleen. The fluorescence from the liver is likely owing to clearance of DiD by the organ. Limbs still showed intense fluorescence even after 12 h injection. In contrast, no fluorescence was detectable in the hind paws of naive rats at any of the time points under the same conditions. These results indicate that polymerized stealth liposomes are able to preferentially accumulate in arthritic joints.

3.5. In vivo therapeutic efficacy

The therapeutic efficacy of polymerized stealth liposomes with Dex, together with PBS and free Dex was studied. Fig. 6a shows the schedule of arthritis induction and treatment regimen. After arthritis was established with obvious swelling and erythema in limbs and paws, they were randomly divided into three groups and then treated with PBS, free Dex and polymerized stealth liposomes with Dex, respectively. The administration frequency was every other day for three injections starting from the 12th

day. Joint score and paw thickness changes during disease progression are crucial parameters to evaluate the anti-inflammatory effect of drugs. Fig. 6b shows the joint score-time curves. Arthritic rats treated with PBS showed increasing joint scores over time as we expected. In contrast, the joint score of arthritic rats treated with free Dex decreased over time. In comparison with free Dex, the decrease of the joint score of arthritic rats treated with polymerized stealth liposomes with Dex was more significant. The therapeutic efficacy of polymerized stealth liposomes with loaded Dex was also examined together with PBS and free Dex based on the paw thickness of arthritic rats. The paw thickness of arthritic rats in each group agreed with the observation of the joint scores (Fig. 6c). Arthritic rats treated with polymerized stealth liposomes with Dex showed the lowest paw thickness. The enhanced therapeutic activity of polymerized stealth liposomes with Dex could be attributed to their long circulation time, preferential targeting at inflamed joints, and high bioavailability.

Pro-inflammatory cytokines such as TNF-α and IL-1β play a crucial role in the progression of joint inflammation.[38] The increase of TNF-α and IL-1β levels can aggravate inflammation diseases, resulting in joint swelling with pain.[39] Thus, we monitored the level of TNF-α and IL-1β in the serum and joint tissues of rats treated with PBS, free Dex and polymerized stealth liposomes with Dex. Naive rats were used as a control group. As can be seen in Fig. 6d-6g, PBS treatments significantly raised the level of TNF-α and IL-1β in both the serum and joint tissues. While the treatment of free Dex and polymerized stealth liposomes with Dex was able to lower the level of TNF-α and IL-1β in both serum and joint tissues. Specifically, the level of TNF-α and

IL-1β after the treatment of polymerized stealth liposomes with Dex was brought down to the level which was close to that of naive rats.

Furthermore, we analyzed the histological pathology of ankle joints using hematoxylin–eosin staining by examining cartilage erosion and cellular infiltration, which are typical features of RA. As can be seen in Fig. 7a, naive rats showed thick cartilage and no cellular infiltration. Compared to the naive rats, the rats treated with PBS had massive cellular infiltration and severe cartilage erosion (Fig. 7b). Although the treatment with free Dex was able to improve joint cartilage because of the anti-inflammatory effect of Dex, intensive cellular infiltration was still observed (Fig. 7c). In contract, the rats treated with polymerized stealth liposomes with Dex exhibited invisible cartilage erosion and limited cellular infiltration (Fig. 7d). The thickness of cartilage in the ankle was comparable to those of naive rats. To further characterize the difference between different treatments, we performed the histological scoring of cartilage erosion and cellular infiltration in a blinded fashion. The histological score was classified by grading the cellular infiltrate and cartilage erosion from 0 to 3 (Figure 7e), where 0 = no; 1 = mild (1%–10%); 2 = moderate (11%–50%); 3 = severe (51%–100%). The rats treated with PBS showed severe cartilage erosion and cellular infiltration (grading from 2 to 3). Moderate cartilage erosion and cellular infiltration were evident in the rats treated with free Dex (grading from 1 to 2). While the rats treated with polymerized stealth liposomes with Dex had minimal cartilage erosion and cellular infiltration (grading below 1) in joints. It is clear that the treatment of polymerized stealth liposomes with Dex is able to alleviate the progression of RA.

Finally, we counted white blood cells (WBC), red blood cells (RBC) and platelets (PLT) after arthritic rats were treated with PBS, free Dex and polymerized stealth liposomes with Dex, together with the count of WBC, RBC and PLT of naive rats (Fig. 8). The rise in the count of WBC and platelets were found in arthritic rats treated with PBS, which correlated with the activity of inflammatory disease. The count of WBC and PLT in arthritic rats was reduced to the normal levels by the treatment of polymerized stealth liposomes with Dex. There was no change in the count of RBC by these treatments.

4. Conclusion

Polymerized stealth liposomes composed $DC_{8,9}PC$ and DSPE-PEG_{2000} were successfully formed through thin-film hydration method followed by UV irradiation to improve the anti-inflammatory efficacy of Dex in the treatment of RA. We demonstrated that the polymerized stealth liposomes were highly stable and showed long blood circulation time. They were biocompatible and could be internalized by cells, especially in inflammatory conditions. After being injected into arthritic rats, the polymerized stealth liposomes were able to accumulate preferentially in inflamed joints. The treatment of polymerized stealth liposomes loaded with Dex sufficiently suppressed the level of proinflammatory cytokines (TNF-α and IL-1β) in joint tissues, reduced the swelling of inflamed joints and alleviated the progression of RA. The good therapeutic activity of Dex could be attributed to the high stability, long blood circulation time, and preferential targeting of polymerized stealth liposomes at inflamed joints.

Acknowledgment

Q. W. acknowledges the support of the Chinese Postdoctoral Science Foundation (Grant No. 2018M640933). J. F. acknowledges the support from the US National Science Foundation (CBET 1803690).

References:

1. G. S. Firestein, *Nature,* 2003, **423**, 356–361.
2. U. Baschant, N. E. Lane, J. Tuckermann, *Nat. Rev. Rheumatol*., 2012, **8**, 645–655.
3. L. K. Prasad, H. O'Mary, Z. Cui, *Nanomedicine,* 2015, **10**, 2063–2074.
4. Q. Wang, X. Sun, *Biomater. Sci.,* 2017, **5**, 1407–1420.
5. M. Yang, X. Feng, J. Ding, F. Chang, X. Chen, *J. Control. Release*., 2017, **252**, 108–124.
6. Z. Fan, J. Li, J. Liu, H. Jiao, B. Liu, *ACS Appl. Mater. Interfaces,* 2018, **10**, 23595−23604.
7. D. Wang, S. R. Goldring, *Mol. Pharm.,* 2011, **8**, 991–993.
8. F. Apparailly, C. Jorgensen, *Nat. Rev. Rheumatol.,* 2013, **9**, 56–62.
9. J. M. van den Hoven, S. R. Van Tomme, J. M. Metselaar, B. Nuijen, J. H. Beijnen, G. Storm, *Mol. Pharm.,* 2011, **8**, 1002–1015.
10. T. M. Allen, P. R. Cullis, *Adv. Drug Deliv. Rev*., 2013, **65**, 36–48.
11. B. S. Pattni, V. V. Chupin, V. P. Torchilin, *Chem. Rev.,* 2015, **115**, 10938–10966.
12. M. Jia, C. Deng, J. Luo, P. Zhang, X. Sun, Z. Zhang, T. A. Gong, *Int. J. Pharm,* 2018, **540**, 57–64.
13. C. R. Alving, E. A. Steck, W. L. Chapman, V. W. Waits, L. D. Hendricks, G. M. Swartz, W. L. Hanson, *Proc. Natl. Acad. Sci. USA,* 1978, **75**, 2959–2963.
14. S. C. Semple, A. Chonn, P. R. Cullis, *Adv. Drug Deliv. Rev*. 1998, **32**, 3–17.

15. D. Papahadjopoulos, T. M. Allen, A. Gabizon, E. Mayhew, K. Matthay, S. K. Huang, K. D. Lee, M. C. Woodle, D. D. Lasic, C. Redemann, *Proc. Natl. Acad. Sci. USA,* 1991, **88**, 11460–11464.

16. V. P. Torchilin, A. L. Klibanov, L. Huang, S. O'Donnell, N. D. Nossiff, B. A. Khaw, *FASEB J.,* 1992, **6**, 2716–2719.

17. A. Gabizon, R. Catane, B. Uziely, B. Kaufman, T. Safra, R. Cohen, F. Martin, A. Huang, Y. Barenholz, *Cancer Res.,* 1994, **54**, 987–992.

18. M. L. Corvo, O. C. Boerman, W. J. G. Oyen, L. Van Bloois, M. E. Cruz, D. J. Crommelin, G. Storm, *Biochim. Biophys. Acta*., 1999, **1419**, 325–334.

19. V. D. Awasthi, D. Garcia, B. A. Goins, W. T. Phillips, *Int. J. Pharm.,* 2003, **253**, 121–132.

20. J. M. Metselaar, M. H. Wauben, J. P. Wagenaar-Hilbers, O. C. Boerman, G. Storm, *Arthritis Rheum*., 2003, **48**, 2059–2066.

21. M. C. Taira, N. S. Chiaramoni, K. M. Pecuch, S. Alonso-Romanowski, *Drug Deliv.,* 2004, **11**, 123−128.

22. C. Boyer, J. A. Zasadzinski, *ACS Nano,* 2007, **1**, 176−182.

23. H. M. Chen, V. Torchilin, R. Langer, *J. Control Release*., 1996, **42**, 263–272.

24. S. Alonso-Romanowski, N. S. Chiaramoni, V. S. Lioy, R. A. Gargini, L. I. Viera, M. C. Taira, *Chem. Phys. Lipids,* 2003, **122**, 191–203.

25. C. Guo, S. Liu, C. Jiang, W. Li, Z. Dai, H. Fritz, X. Wu, *Langmuir,* 2009, **25**, 13114–13119.

26. A. Yavlovich, A. Singh, R. Blumenthal, A. Puri, *Biochim. Biophys. Acta,* 2011, **1808**, 117–126

27. H. F. Li, C. Wu, M. Xia, H. Zhao, M. X. Zhao, J. Hou, R. Li, L. Wei, L. Zhang, *RSC Adv*., 2015, **5**, 27630–27639.

28. J. Leaver, A. Alonso, A. A. Durrani, D. Chapman, *Biochim. Biophys. Acta.,* 1983, **732**, 117–126.

29. N. Mahajan, R. Lu, S. T. Wu, J. Y. Fang, *Langmuir,* 2005, **21**, 3132–3235.

30. M. Kastantin, B. Ananthanarayanan, P. Karmali, E. Ruoslahti, M. Tirrell, *Langmuir* 2009, **25**, 7279–7286.

31. D. C. Litzinger, A. M. Buiting, N. van Rooijen, L. Huang, *Biochim. Biophys. Acta* 1994, **1190**, 99–107.

32. H. Ren, Y. He, J. Liang, Z. Cheng, M. Zhang, Y. Zhu, C. Hong, J. Qin, X. Xu, J. Wang, *ACS Appl. Mater. Interfaces,* 2019**, 11**, 20304–20315.

33. D. Koley, A. J. Bard, *Proc. Natl. Acad. Sci. USA.,* 2010, **107**, 16783–16787.

34. C. Kirby, G. Gregoriadis, *Biochem. J.* 1981, **199**, 251–254.

35. C. Kirby, J. Clarke, G. Gregoriadis, *FEBS Lett*., 1980, **111**, 324–328.

36. T. Ishida, H. Harashima, H. Kiwada, *Biosci. Rep*., 2002, **22**, 197–224.

37. L. Quan, Y. Zhang, B. J. Crielaard, A. Dusad, S. M. Lele, C. J. F. Rijcken, J. M. Metselaar, H. Kostkova, T. Etrych, K. Ulbrich, F. Kiessling, T. R. Mikuls, W. Hennink, G. Storm, T. Lammers, D, Wang, *ACS Nano,* 2014, **8**, 458–466.

38. C. A. Dinarello, *Chest,* 2000, **118**, 503–508.

39. E. H. Choy, G. S. N. Panayi, *Engl. J. Med*., 2001, **344**, 907−916.

Figure Captions

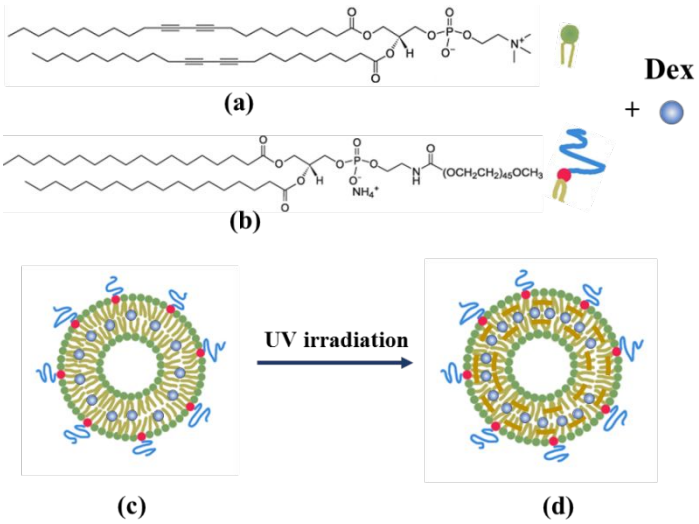

Fig. 1: Chemical structure of $DC_{8,9}PC$ (a) and DSPE-PEG_{2000} (b). Schematic of nonpolymerized (c) and polymerized (d) stealth $DC_{8,9}PC$/DSPE-PEG_{2000} liposomes with loaded Dex.

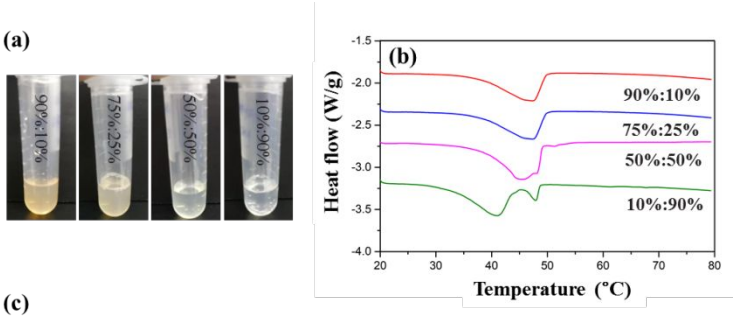

(c)

$DC_{8,9}PC$:DSPE-PEG_{2000} (Molar ratio%)	Size（nm）	PDI
90:10	121.4 ± 9.8	0.24 ± 0.08
75:25	139.4 ± 5.8	0.25 ± 0.12
50:50	196.0 ± 8.7	0.36 ± 0.11
10:90	185.2 ± 12.1	0.46 ± 0.17

Fig. 2: (a) Photography images of polymerized stealth liposome solution. (b) Differential scanning calorimetry of polymerized stealth liposomes. (c) Size and PDI value of polymerized stealth liposomes.

(a)

	Size (nm)	Zeta potential	Encapsulation rate (%)	Drug loading yield (%)
Non-polymerized liposomes	134.7 ± 6.5	-17.1 ± 4.2	16.7 ± 3.2	3.5 ± 0.6
Polymerized liposomes	121.4 ± 9.8	-18.0 ± 3.6	85.0 ± 6.4	17.1 ± 1.2

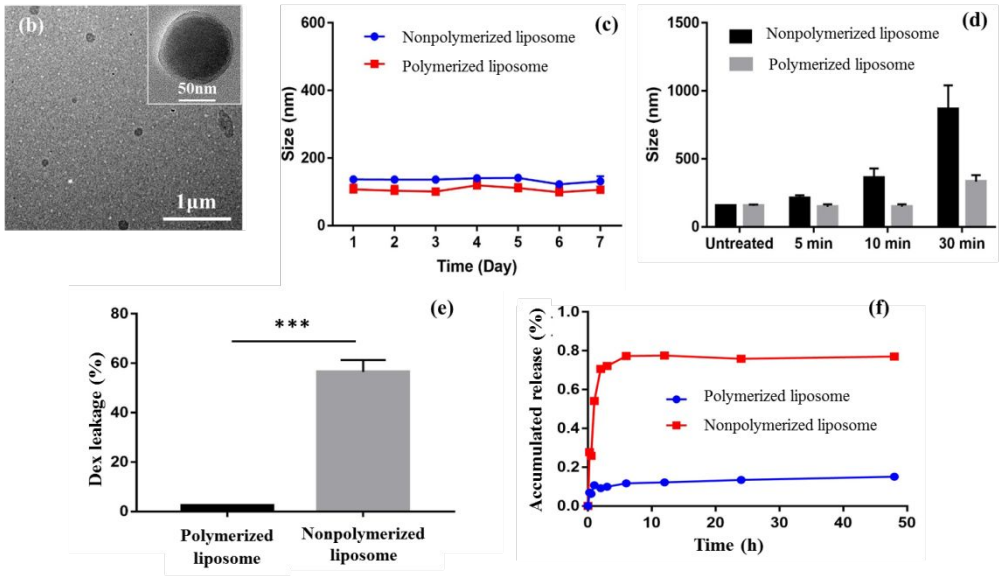

Fig. 3: (a) Size, Zeta potential, encapsulation rate and drug loading yield of polymerized and nonpolymerized stealth liposomes. (b) TEM image of polymerized stealth liposomes. The inset in b is a magnified image of a single liposome. Size of polymerized and nonpolymerized stealth liposomes in aqueous solution at room temperature without (c) and with (d) 20 μM Triton X-100 at different time intervals. (e) Dex leakage of polymerized and nonpolymerized stealth liposomes after being incubated with serum for 4 h. Results were shown as mean ± SD, n= 3, ***p< 0.001. (f) In vitro release behaviors of Dex from polymerized and nonpolymerized stealth liposomes in PBS solution.

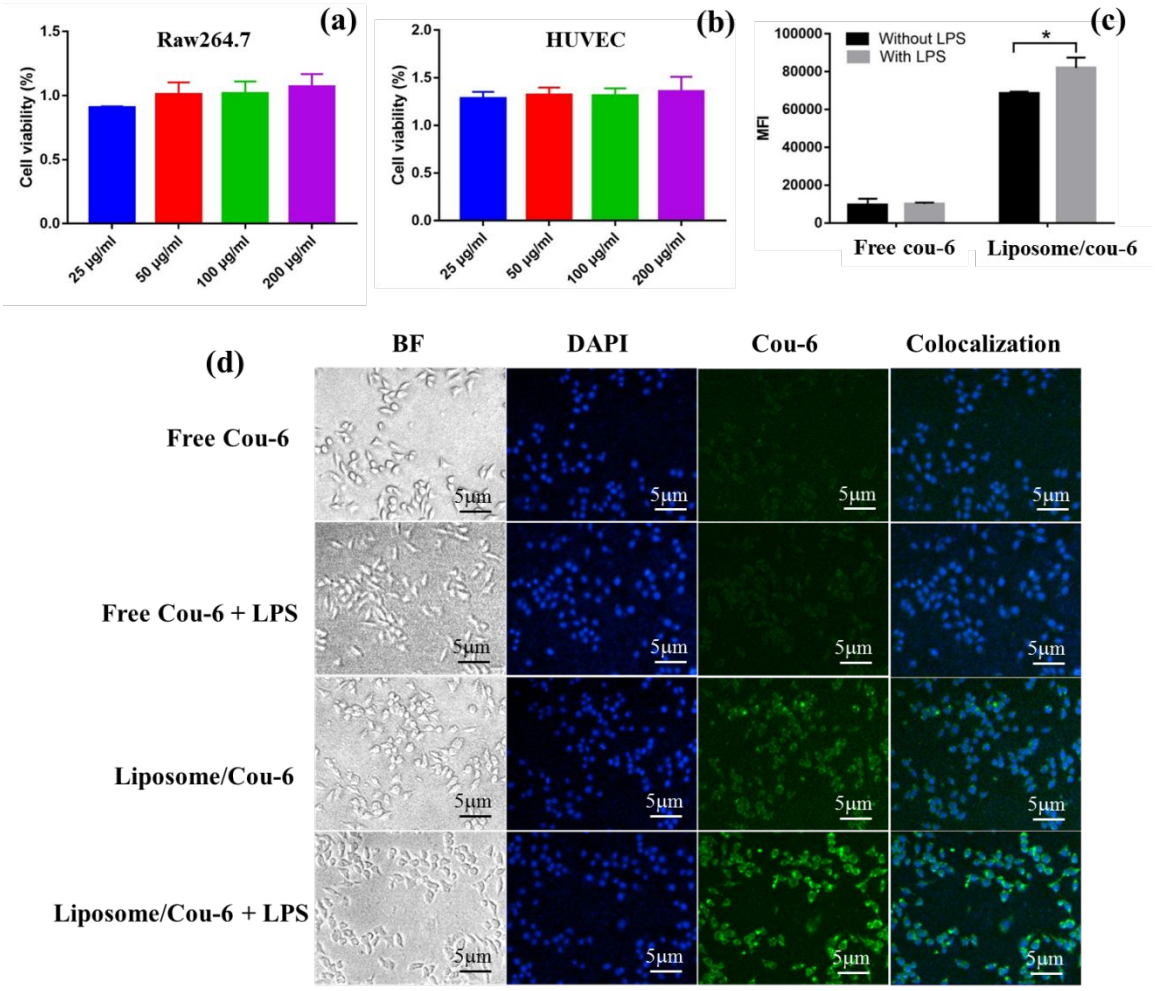

Fig. 4: Viability of Raw 264.7 (a) and HUVEC (b) cells after 24 h incubation with polymerized stealth liposomes. Mean fluorescence intensity (MFI) (c) and fluorescence microscopy images (d) of cellular uptake of free Cou-6 and polymerized stealth liposomes with loaded Cou-6 by Raw264.7 with and without the presence of LPS. Results in a, b, and c were shown as mean ± SD, n= 3, *p< 0.05. Cell nucleus were stained with DAPI (blue). BF: bright field. Cou-6: Couramin-6.

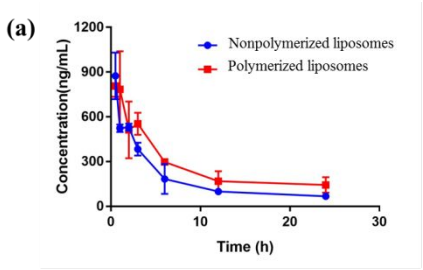

(b)

	Non-polymerized liposomes	Polymerized liposomes
AUC (μg/L*h)	5889 ± 350	10226 ± 426
$T_{1/2}$ (h)	6.11 ± 1.98	9.53 ± 1.24

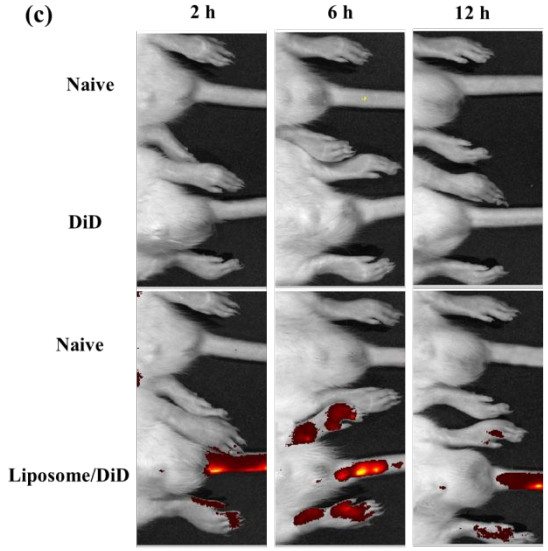

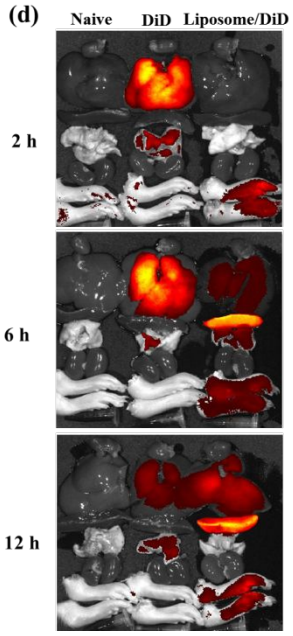

Fig. 5: (a) Pharmacokinetics profiles after intravenously injecting polymerized and non-polymerized stealth liposomes at the dose of 2 mg/kg. Results were shown as mean ± SD, n = 6. (b) AUC (area under the concentration-time curve) and $T_{1/2}$ (half-life). These pharmacokinetic parameters were calculated by DAS software. (c) Biodistribution of rats after the intravenous injection of free DiD or polymerized stealth liposomes with loaded DiD at different time points. (d) Ex vivo images of main tissues at different time points. From top to bottom: heart, liver, spleen, lung, kidney, and limbs. Naive rats served as the control group to deduct the autofluorescence of rats.

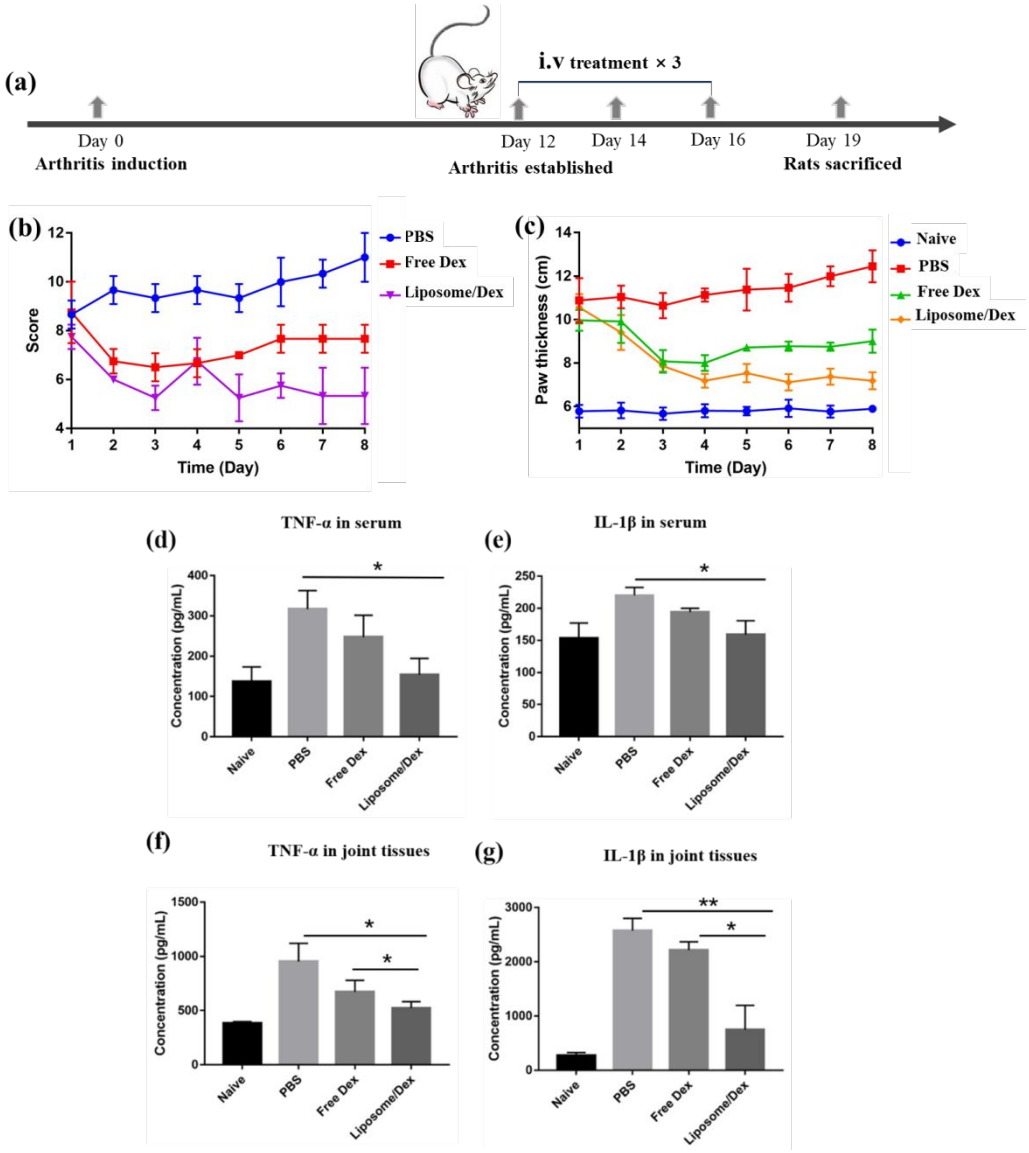

Fig. 6: (a) Time schedule of arthritis induction and therapeutic treatment. (b) Joint score and (d) paw thickness after the treatment of PBS, free Dex, and polymerized stealth liposomes with loaded Dex. Inflammatory levels of TNF-α and IL-1β in serum (d, e) and joint tissues (f, g) after the treatment of PBS, free Dex and polymerized stealth liposomes with Dex. Naive rats served as the control group. Results were shown as mean ± SD, n = 6. *p< 0.05, **p< 0.01.

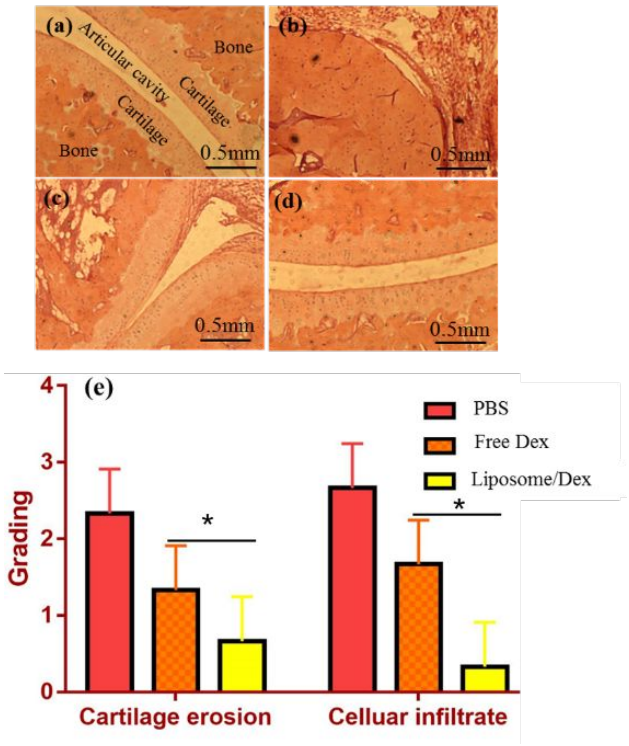

Fig. 7: Representative histological images of ankle joints of naive rats (a), and rats treated with PBS (b), free Dex (c) and polymerized stealth liposome with Dex (d). (e) Histological scores of cartilage erosion and cellular infiltration after the treatment of PBS, free Dex and polymerized stealth liposomes with Dex. Results were shown as mean ± SD, n = 5. *p< 0.05.

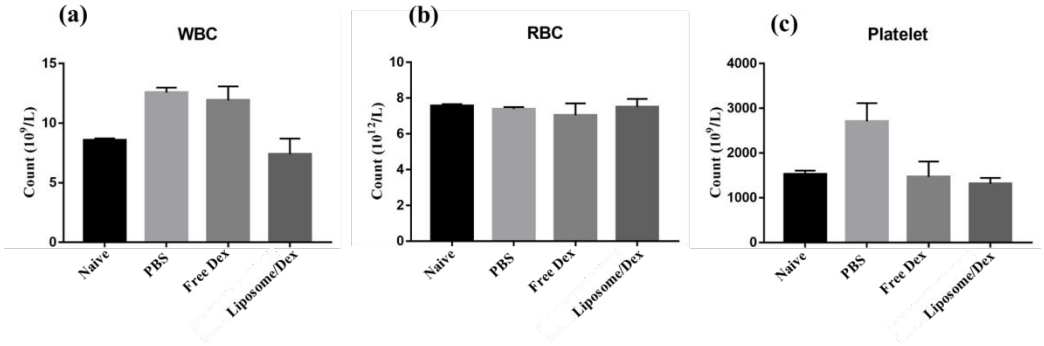

Fig. 8: (a) WBC, (b) RBC, and (c) platelet counts after the treatment of PBS, free Dex and polymerized stealth liposomes with Dex. Naive rats served as the control group. Results were shown as mean ± SD, n = 6.

The table of contents

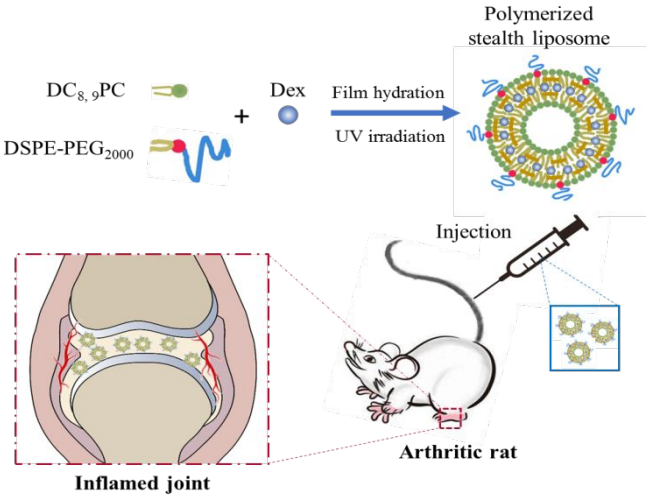

Polymerized stealth liposomes were developed for improving the anti-inflammatory efficacy of dexamethasone in the treatment of rheumatoid arthritis.